E. M. Ortt[1]
Assoc. Mem. ASME

D. J. Doss[1]
Assoc. Mem. ASME

E. Legall

N. T. Wright
Mem. ASME

J. D. Humphrey[2]
Mem. ASME

Department of Mechanical Engineering,
University of Maryland,
Baltimore, MD 21250

A Device for Evaluating the Multiaxial Finite Strain Thermomechanical Behavior of Elastomers and Soft Tissues

Described here is the design and development of a computer-controlled device capable of measuring the finite strain thermomechanical behavior of a general class of polymeric materials including elastomers and biological soft tissues. The utility of this device for thermoelastic and thermophysical investigations is demonstrated by the measurement of the in-plane stress-stretch response and in-plane and out-of-plane components of thermal diffusivity of neoprene rubber undergoing finite deformations. [S0021-8936(00)01603-2]

Introduction

The thermomechanical behavior of elastomeric, and specifically rubber-like, materials has generated considerable interest in the mechanics community for close to two centuries. With the advent of laser, ultrasound, and microwave-based medical devices, a similar interest has recently arisen in the thermomechanical behavior of soft tissues ([1]). A general thermomechanical analysis of these material behaviors requires, of course, both multiaxial thermoelastic and thermophysical data. Likewise, formulation of nonlinear constitutive relations necessitates appropriate theoretical frameworks to design and interpret the requisite experiments ([2]). For example, theory reveals that a complete description of reversible finite strain thermomechanical behavior requires identification of two independent constitutive functions ([3]), the Helmholtz potential

$$\psi = \hat{\psi}(\mathbf{C}, T), \tag{1}$$

and the referential heat flux vector

$$\mathbf{q}_0 = \hat{\mathbf{q}}_0(\mathbf{C}, T, \nabla_0 T), \tag{2}$$

where $\mathbf{C}\,(=\mathbf{F}^T\cdot\mathbf{F})$ is the right Cauchy-Green deformation tensor, $\mathbf{F}\,(=\partial\mathbf{x}/\partial\mathbf{X})$ the deformation gradient tensor, T the temperature, $\nabla_0 T\,(=\partial T/\partial\mathbf{X})$ the referential temperature gradient, and $\mathbf{x}$ and $\mathbf{X}$ the position of a material particle in the current and reference configurations, respectively. Stress-strain-temperature relations result from derivatives of $\hat{\psi}$ with respect to $\mathbf{C}$. Although a number of functional forms for $\hat{\psi}$ have been suggested ([4–7]), a widely accepted form remains elusive due, in large part, to the continuing lack of multiaxial thermoelastic data. That is, most investigators have focused on describing the available uniaxial data ([8–11]) and hence the peculiar one-dimensional Gough-Joule and thermoelastic inversion effects. Recently, however, Ogden [7] proposed a method for finding $\hat{\psi}$ as a function of biaxial stretches and temperature, whereas Humphrey and Rajagopal [12] showed that in-plane biaxial tests allow measurement of thermoelastic response functions (e.g., $\partial\hat{\psi}/\partial I_C$ where $I_C=\mathrm{tr}\,\mathbf{C}$) similar to the isothermal results of Rivlin and Saunders [13]. Both cases require measuring biaxial stress and stretch at multiple temperatures.

Alternatively, there has been little attention to the possible finite strain dependence of the heat flux. Rather, most reports assume Fourier conduction $\mathbf{q}(\mathbf{x},T)=-k(T)\nabla T$ where $\mathbf{q}(\mathbf{x},T)$ is the spatial heat flux, $\nabla T\,(=\partial T/\partial\mathbf{x})$ the spatial gradient of temperature, and $k(T)$ the scalar (i.e., isotropic) spatial thermal conductivity ([14]). For finite strains, referring the conductivity tensor to the reference configuration simplifies material symmetry considerations, and thereby facilitates the formulation of general constitutive relations. Thus, note that $\mathbf{q}=(1/J)\mathbf{F}\cdot\mathbf{q}_o$, where $J=\det\mathbf{F}$. Moreover, a generalized Fourier conduction has the form

$$\mathbf{q}(\mathbf{x},T)=\frac{1}{J}\mathbf{F}\cdot(-\mathbf{K}(\mathbf{C},T)\cdot\nabla_0 T(\mathbf{X},T)) \tag{3}$$

where $\mathbf{K}(\mathbf{C},T)$ is the referential thermal conductivity tensor. Of the tractable finite strain tests (e.g., combined extension and torsion of a cylinder, membrane inflation, etc.), the in-plane biaxial extension of a thin rectangular sheet ([13,15]) is also convenient for thermophysical testing. Not only is the resulting strain field homogeneous in the central region and the state of stress planar, thin specimens facilitate isothermal testing and measurement of thermal diffusivity. For example, Doss and Wright [16] recently demonstrated that the transient flash diffusivity method ([17]) may be extended to measure the diagonal components of the spatial thermal diffusivity tensor $\boldsymbol{\alpha}$ of thin sheets of stiff polyvinyl chloride (PVC). Specifically, the flash diffusivity method yields $\boldsymbol{\alpha}$ via the spatial energy equation which, in the absence of stress power and volumetric heat addition, is

$$\frac{dT(\mathbf{x},T)}{dt}=\boldsymbol{\alpha}(\mathbf{C},T):\nabla(\nabla T(\mathbf{x},t)) \tag{4}$$

where t is time. For materials in mechanical equilibrium, the convective terms within the material are negligible, of course, and the total derivative on the left-hand side of Eq. (4) reduces to a partial derivative with respect to time. Appendix A contains an outline of the one-dimensional solution of Eq. (4) that Parker et al. [17] employed in the initial description of the flash method. Here, Eq. (4) is solved using a finite difference formulation as part of a Marquardt parameter estimation algorithm for both the traditional (one-dimensional) flash method (measuring the out-of-plane component α_{33} only) and the extended flash method (measuring the three diagonal components of $\boldsymbol{\alpha}$). This allows for more accurate representation of the boundary conditions. Appendix A also outlines this model. Regardless, note that finite strain constitutive relations are more easily formulated in terms of the referential

[1]Current address: Black & Decker, Inc., 701 E. Joppa Road, Towson, MD 21286.
[2]To whom correspondence should be addressed. Biomedical Engineering Program, Texas A&M University, 233 Zachry Engineering Center, College Station, TX 77843-3120. E-mail: jdh@acs.tamu.edu

Contributed by the Applied Mechanics Division of THE AMERICAN SOCIETY OF MECHANICAL ENGINEERS for publication in the ASME JOURNAL OF APPLIED MECHANICS. Manuscript received by the ASME Applied Mechanics Division, Apr. 21, 1999; final revision, Dec. 13, 1999. Associate Technical Editor: K. T. Ramesh. Discussion on the paper should be addressed to the Technical Editor, Professor Lewis T. Wheeler, Department of Mechanical Engineering, University of Houston, Houston, TX 77204-4792, and will be accepted until four months after final publication of the paper itself in the ASME JOURNAL OF APPLIED MECHANICS.

thermal diffusivity $\boldsymbol{\alpha}_0$. Fortunately, one can infer $\boldsymbol{\alpha}_0$ from the measurable $\boldsymbol{\alpha}$ via $\boldsymbol{\alpha}=(1/J)\mathbf{F}\cdot\boldsymbol{\alpha}_0\cdot\mathbf{F}^T$ where $\boldsymbol{\alpha}_0(\mathbf{C},T)=\mathbf{K}(\mathbf{C},T)/(\rho_0 c_F(\mathbf{C},T))$; here ρ_0 is the referential mass density and c_F the specific heat at constant deformation.

There is, therefore, a clear need for a multiaxial thermomechanical test system that can exploit the available theoretical results. This paper describes the design and construction of a new device capable of both in-plane biaxial thermoelastic testing and measurement of the orthogonal components of $\boldsymbol{\alpha}$. Illustrative data are presented for neoprene subject to equibiaxial stretch ratios $\lambda \equiv \lambda_1=\lambda_2$ ($\lambda_i=l_i/L_i$, no sum on i, with l_i and L_i being current and reference lengths, respectively) with $\lambda\in[1,1.5]$, at temperature levels of 21 and 41°C.

Experimental System

Figure 1 is a schema of the overall optical-thermomechanical system. The system consists of five subsystems, one each for (a) biaxial loading, (b) in-plane strain measurement, (c) environmental control, (d) flash illumination, and (e) point-wise temperature measurement.

Biaxial Loading System. The load frame is machined from one piece of mild steel to outer dimensions of 45.7×45.7 cm with a 2.54 cm square cross section. The outer and inner surfaces are ground to ensure that opposing sides are flat and parallel. The frame is mounted on an optical table using a standard 2.54-cm diameter, 15.2-cm long support rod at each corner. A pair of horizontal through-holes (1.27-cm diameter and 4.45 cm apart) are centered on each side of the frame (Fig. 2(*a*)) such that the axes of any pair of holes are collinear with those of the opposing pair and perpendicular to the other two pairs. Each of the eight holes is fitted with a 1.91-cm-long linear recirculating ball bearing specifically designed for linear travel of shafts with minimal transverse play.

Nearly uniformly distributed in-plane biaxial forces are applied to the square specimen through four load carriages (Fig. 2(*b*)). Each edge of the specimen is attached to a single carriage using Kevlar thread (or silk suture for biological tissues). The load carriages consist of two parallel 0.635-cm-diameter solid, hardened stainless steel rods. Each rod is supported in one of the aforementioned through-holes by one of the linear bearings in the load frame and a neoprene O-ring sandwiched between two Rulon bearings, which form a watertight seal for the environmental chamber. Proper alignment of this chamber within the load frame ensures free and smooth translation of the load carriages. The outside end of each pair of rods is attached to a cross bar that separates the shafts and facilitates the application of axial forces. The inside end of each load carriage consists of three separate aluminum pieces: a cross bar that connects the two rods, a coupling bar, and a T-bar that has a series of equally spaced holes (0.75 cm apart) that serve as rigging points for the specimen loading threads. Two of the load carriages, one on each axis, have watertight and temperature compensated ($T\in[-29,93]$°C) load cells mounted between the cross bar and coupling bar.

The last component of the loading subsystem is the mechanism for inducing axial load. Each of the four carriage assemblies is independently loaded via a 1-mm lead ball-screw driven by a stepper motor. A ball-nut attached to the outer cross bar of each load carriage converts the rotation of the ball-screw into linear displacement of the carriage assembly. The stepper motors are individually controlled by a four-axis indexer card in the Pentium personal computer (PC). Such a drive system allows implementation of fully automated stretching protocols.

Strain Measurement. In-plane finite strains are measured optically by tracking the position histories of four small, contrasting markers that are affixed to the bottom surface of the specimen (Fig. 2(*b*)). This approach has been described previously ([18]), and is sufficient because of the homogeneity of the strain field in the central region, as confirmed via pilot experiments as well as by finite element analysis. For example, finite element analysis (ABAQUS), assuming a Mooney-Rivlin material response, revealed that the strain field is essentially homogeneous and extensional (< 5 percent shear) in the central sixteenth of the planar area of a square elastomeric specimen ([19]) that is loaded by five equidistant point loads at each edge. A CCD video camera, frame-grabber board in the PC, and custom software track the position of each of the four markers at the 30 Hz frame rate. The software algorithm, based on Downs et al. [20], uses a correlation method to locate the markers first in a ''coarse'' and then in a ''fine'' search region. The marker positions serve as input to a bilinear isoparametric interpolation algorithm that provides the components of **F** in the central region at each configuration (see Appendix B). The components of **F** provide information for feedback control (described below) of the thermoelastic tests at thermal equilibrium. In thermophysical tests, the components of **F** are reg-

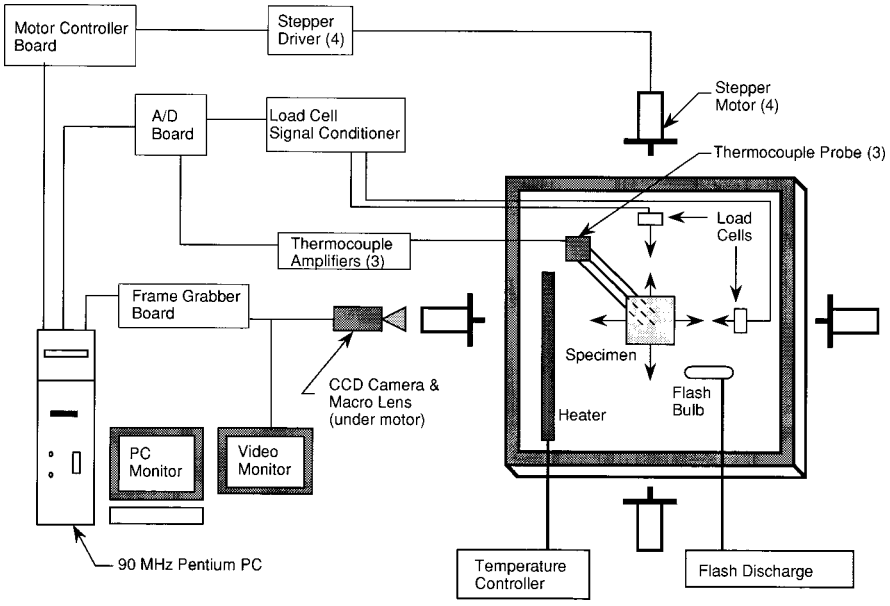

Fig. 1 A schematic drawing of the overall experimental system

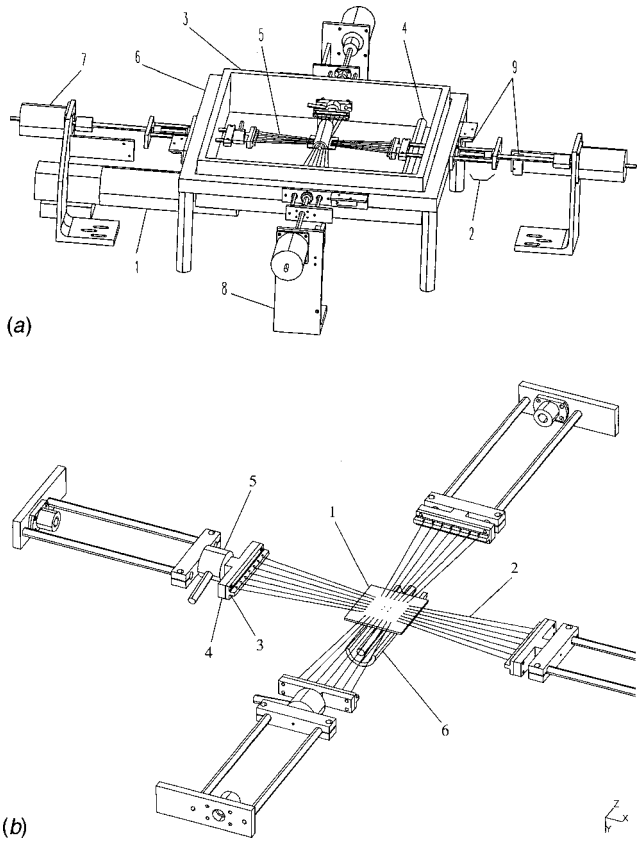

Fig. 2 Biaxial extension device. Panel (a) is an oblique view of the device where (1) camera, (2) load carriage, (3) environmental chamber, (4) heater, (5) Kevlar threads, (6) load frame, (7) motors, (8) motor supports, and (9) limit switches; in-plane directions defined as 1 and 2. Panel (b) is a schema of (1) the specimen with centrally placed tracking markers, (2) Kevlar threads, (3) T-bar, (4) coupling bar, (5) load cell, and (6) flashbulb and reflector, as seen from below.

istered prior to the flash illumination (i.e., at mechanical equilibrium), which only slightly perturbs the strain field.

Environmental Chamber. The environmental chamber allows testing of the sample in air or liquid at nearly constant temperatures (± 1°C). The chamber is constructed from a 1.27-cm-thick polycarbonate sheet and sealed with silicone adhesive to prevent leakage of the solution. With outside dimensions $40.0 \times 40.0 \times 7.62$ cm, the polycarbonate shell fits inside of the load frame (Fig. 2(*a*)). Though not shown for clarity, top and bottom plates are screwed onto the polycarbonate shell and silicone rubber gaskets form seals between the plates and shell.

The top plate of the chamber has a central port that allows the flash lamp (described below) to be placed in close proximity to the specimen, thereby ensuring that enough energy is absorbed by the sample to obtain a desirable temperature rise on its bottom surface. The separation between the lamp and an approximately 2-mm-thick specimen may be adjusted between 1.0 and 3.0 cm. In addition, the top plate allows access by the thermocouple probe for measurement of the temperature field on the bottom face of the sample. The bottom plate has a central $96 \times 96 \times 1.5$ mm glass window that allows the camera to view the aforementioned markers for strain measurement. Additionally, the bottom plate has drains to remove liquid from the chamber.

The chamber can be maintained between room temperature and 90°C by a 750 W, 1.27-cm-diameter, 30.5-cm-long submersible heater that is mounted in the chamber (Fig. 2(*a*)) and modulated by a thermostatic controller.

Temperature Measurement and Flash System. The principle of the flash technique for measuring thermal diffusivity is described elsewhere ([21–23,17,24]). Briefly, a flash system consists of a radiant energy source (e.g., a flash lamp or pulsed laser) capable of delivering a short burst that heats one face of the specimen, and a probe to measure the associated temperature history on the opposite face. Here, a linear xenon flashtube, mounted in an aluminum reflector, illuminates the top face of the specimen. When the in-plane components of $\boldsymbol{\alpha}$ are to be measured, a 50×50 mm aperture plate with a central 20×20 mm opening is mounted between the source and the specimen; the aperture is removed for measurement of α_{33} alone. Three 0.25-mm-diameter E-type thermocouple probes are mounted in an aluminum bar and form the apexes of a right isosceles triangle having two 15-mm sides, and when aligned with the aperture, they measure the temperature at the center of the projection of the lighted area and at two points outside this projection along the two in-plane axes. For measurements of α_{33} alone, only the central thermocouple output need be used. A small amount of high thermal conductivity silicone paste is used to insure good contact between the thermocouple probe and the specimen surface. The fixture is attached, through the port in the top plate of the environmental chamber, to a micrometer head that can raise or lower the thermocouples as required. A second CCD camera and mirror (not shown) monitors the contact between the specimen and the thermocouples.

Data Acquisition and Control. Eight independent channels of information are recorded simultaneously using an analog-to-digital (A/D) conversion board in the PC. The A/D board has high-gain amplification and a cold junction compensation circuit, specifically designed for acquisition of thermocouple data, recorded on one of the eight channels. The E-type thermocouples occupy three channels, whereas two T-type thermocouples, one at the glass window covering the flashbulb to mark the flash event on the data file and another above the specimen to record the ambient temperature, occupy two channels. The two load cells are connected to a signal conditioner, the output of which occupies the last two channels.

The strategy to control the biaxial finite deformation involves actuating the two opposing motors in one stretching direction at a constant velocity and varying the velocity of the two motors in the orthogonal direction so that the measured stretch in that direction is within a small error ϵ of the desired stretch. Hence, let λ_d be the desired stretch (either λ_1 or λ_2), λ_a be the measured stretch, and δ the difference between λ_a and λ_d. If $|\delta| \leq \epsilon$, then the velocities of the two motors on that axis are set to zero. If $|\delta| > \epsilon$, however, then the motor velocities must be adjusted to bring λ_a back to within ϵ of λ_d. The velocities ω of the controlled motors are adjusted proportionally to δ using $\omega = G\delta$, where G is a suitably valued parameter determined by trial and error during preliminary tests until the control of the specimen is acceptable. If G is too small, the stepper motors move continuously in the same direction, indicating that ω is too low and possibly not keeping the stretches within ϵ. Conversely, if G is too large, the motors oscillate, indicating an overshoot of λ_d, thus requiring the motors to reverse. A suitable value of G between these two extremes should thus be selected. Note that if $\delta > 0$, then $\lambda_a > \lambda_d$ and the direction of rotation of the motors must be such that λ_a is decreased; if $\delta < 0$ then the specimen must be stretched more. Once the controlling velocity is determined, its value is sent to the motor controller card. The control cycle is repeated throughout the experiment at 30 Hz by calculating the new stretch ratios, determining the controlling velocity, and sending the new velocity to the motor controller card.

Specimen Preparation. Thermoelastic tests were performed on specimens measuring 50-mm square cut from 1.6-mm-thick precast sheets of high-grade neoprene rubber with a Shore A hardness value of 35–45 (McMaster Carr). Outside of the biaxial device, each edge of the specimen was sewn to a T-bar using a

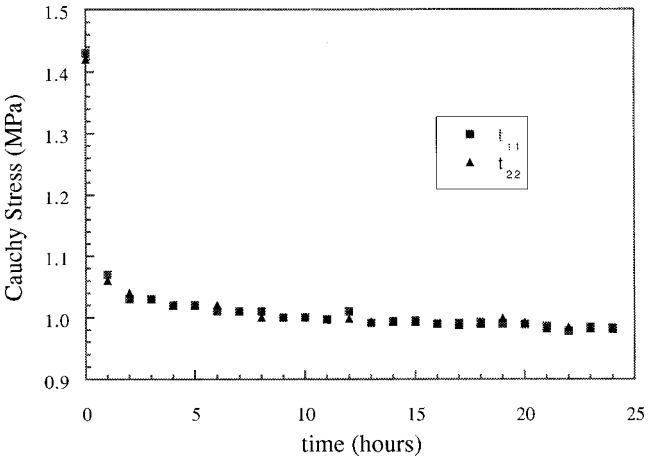

Fig. 3 Stress relaxation curve of a neoprene rubber specimen during preconditioning

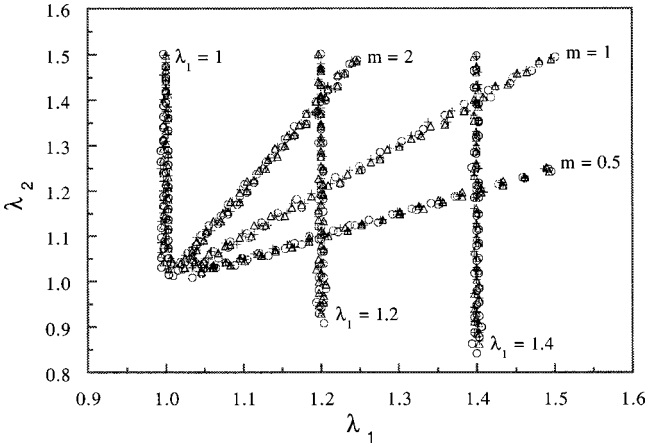

Fig. 4 Illustrative in-plane stretches λ_1 and λ_2 for computer controlled equibiaxial, proportional, and constant λ_1 stretching protocols. Data are for three cycles each (cycle 1: +, 2: △, 3: ○), thus showing reproducibility and robust control.

0.254-mm-diameter sewing needle and 0.2-mm-diameter Kevlar thread. Six holes spaced about 3.75 mm apart and 10 mm from the edge of the specimen were used on each edge. Four white 200-μm spots of titanium white acrylic paint were placed in the central 5×5 mm square (i.e., 1/100th of the planar area) of the specimen on the bottom face of the black specimen. The T-bars were then attached to the coupling bars (Fig. 2(*b*)). Prior to thermoelastic testing, each specimen was systematically preconditioned, thermally and mechanically: each neoprene sample was held at an in-plane equibiaxial stretch ratio of $\lambda=1.45$ at 41°C for 24 hours. The reduced range of temperatures examined in these first measurements on neoprene, as compared with the 90°C capability of the chamber, are the result of the reduced tear resistance of neoprene at elevated temperatures. Figure 3 shows the stress relaxation response of a typical specimen during preconditioning. The relaxation response was 86 percent complete after two hours and more than 95 percent complete after 12 hours. Immediately following the 24 hours of such preconditioning, the sample was unloaded and subjected to thermoelastic testing. Preconditioning for the thermophysical tests was similar. New specimens were preconditioned at an equibiaxial stretch of $\lambda=1.52$ at 25°C for 16 hours.

Illustrative Results

Stress-Strain Response. Figure 4 illustrates the ability of the system to execute well the prescribed protocols in (a) constant λ_1 tests, with $\lambda_1=1$, 1.2, 1.4, and (b) proportional stretch tests where $(\lambda_2-1)/(\lambda_1-1)=m$, with $m=2$, 1, 0.5; equibiaxial stretch is a special case with $m=1$. Each of the tests consisted of three cycles at a frequency of about 0.017 Hz. The repeatability over the three cycles for each type of test illustrates the robust control and the effect of preconditioning. Recall that the automated control of the motors was based on the video strain measurement of the in-plane stretches, thus permitting corrections at 30 Hz.

For homogeneous principal extensions $\mathbf{F}=\mathrm{diag}[\lambda_1,\lambda_2,\lambda_3]$ and $J=\det\mathbf{F}=\lambda_1\lambda_2\lambda_3=\rho_0/\rho$ (where ρ_0 and ρ are the reference and current mass densities, respectively), hence λ_3 can be determined at each temperature, given $\rho=\rho(T)$. Data obtained from Anter Laboratories (Pittsburgh, PA) on neoprene samples tested at $T\in[20,60]$°C suggest that, to first order,

$$\rho(T)=\rho_0[1+\beta(T-T_0)]^{-1} \tag{5}$$

where $\rho_0=1.317\ \mathrm{g/cm^3}$, $\beta=3.915\times10^{-4}(°\mathrm{C})^{-1}$, and $T_0=20$°C is the reference temperature at which ρ_0 is measured. Figure 5 shows illustrative in-plane Cauchy stress as a function of modified stretch ratio $\lambda_1^*(=J^{-1/3}\lambda_1)$ for one sample at three temperature levels ($T=25,33.2,41.2$°C). The stretches are calculated in the central region of the specimen with respect to the stress-free reference configuration at the reference temperature. The characteristic nonlinear behavior is well known and has been well documented in the past ([8,25,26,11]). Similar measurements on specific materials of interest will add greatly to the existing thermoelastic database that is needed to evaluate current constitutive thermoelastic models ([5,12,7]) as well as to develop new constitutive descriptors of other such materials.

Thermal Diffusivity. Two types of tests illustrate the ability of the device to measure thermal diffusivity of specimens subjected to finite in-plane deformation: measurements of (a) α_{33} for three specimen thicknesses and multiple equibiaxial stretches and (b) the diagonal components of $\boldsymbol{\alpha}$ as a function of finite equibiaxial deformation at room temperature.

First, α_{33} was measured for three neoprene specimens of nominal thicknesses of 1.6, 2.4, and 3.2 mm. Following preconditioning and then registration of the unloaded reference configuration (i.e., recording the marker positions) at $T_0\approx21$°C (i.e., ambient room temperature), the top surface of each specimen was subjected to a series of five pulses from the flash lamp, each separated by ten minutes to allow the specimen to regain thermal equilibrium. Figure 6 shows a typical bottom surface temperature response following the flash. For a bottom surface temperature T_b,

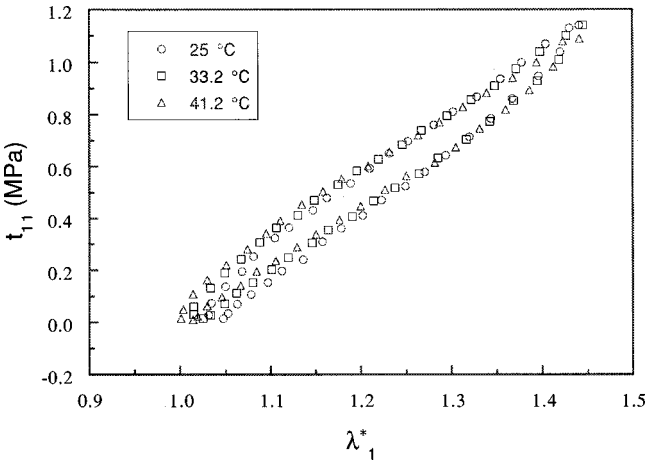

Fig. 5 Typical Cauchy stress-stretch curves for neoprene at three temperatures for equibiaxial stretch tests

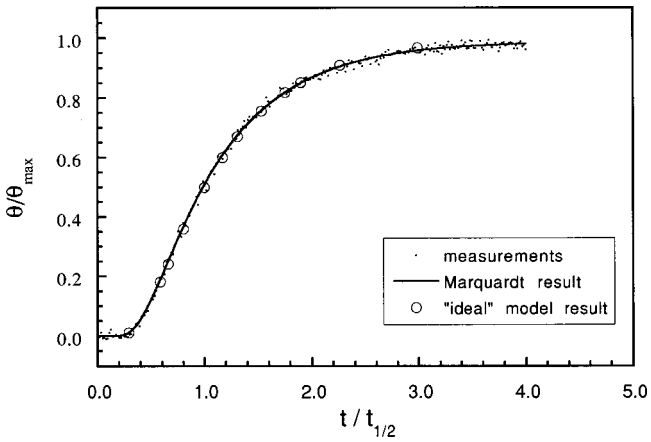

Fig. 6 Bottom surface temperature history for a one-dimensional flash test showing the close agreement between the measurements, the temperature history calculated as part of the data reduction, and that calculated assuming the boundary conditions originally used by Parker et al. [17] and the value of α_{33} determined by the Marquardt data reduction. $\tau_{1/2} \approx 4$ s.

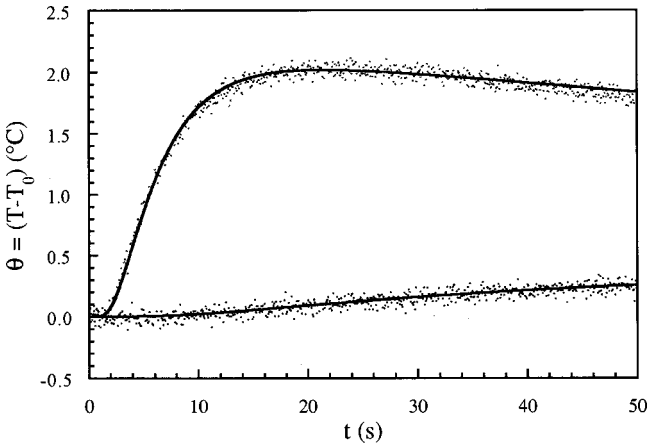

Fig. 7 Temperature history of the central and one of the lateral thermocouples for equibiaxial in-plane stretch of $\lambda = 1.03$. Solid line is model result.

the temperature excess $\theta = T_b - T_0$ has been scaled by the maximum temperature excess measured on the bottom surface $\theta_{\max}$ (typically about 3°C). Time has been scaled by $t_{1/2}$ (typically about 4 s), which is the time at which the bottom surface reaches $\theta_{\max}/2$. After the five pulses, the specimen was extended equibiaxially to the next desired stretch, its marker positions recorded in this equilibrium configuration following stress relaxation, and the flash procedure repeated. Once all data were collected at room temperature, another series of stretch and flash data were collected at 40°C. After increasing the temperature level, the sample was allowed to reach thermal equilibrium prior to inducing mechanical stretch.

Since the transient temperature rise on the bottom surface due to each flash was about 3°C and of similar magnitude on the top face, after a brief initial transient (10 ms), data were collected at nearly mechanical and thermal equilibrium. Here, the bottom surface temperature history was measured directly and α_{33} was calculated using the Marquardt parameter estimation algorithm coupled with a finite difference solution of Eq. (4) outlined in Appendix A. Figure 6 shows close agreement between the measurements, the temperature history calculated as part of the data reduction, and that calculated assuming the boundary conditions originally used by Parker et al. [17] and the value of α_{33} determined by the Marquardt data reduction. The mean values of α_{33} found in these one-dimensional measurements are 0.119 mm^2/s at 21°C and 0.117 mm^2/s at 40°C. These values are within five percent of those measured by Anter Labs and match well the trend with temperature, though this decrease is within the scatter of the measurements and thus, not statistically significant.

A second set of tests measured the diagonal components of $\boldsymbol{\alpha}$ for three specimens with a nominal thickness of 2.4 mm. Again, following preconditioning, each specimen was tested at two equibiaxial stretch states of approximately $\lambda = 1.03$ and 1.52. A minimum of five flash tests were performed at each of the two deformation states. Figure 7 shows the measured bottom-surface temperature history of a typical test along with the best-fit results based on the three-dimensional finite difference model. Again, there is close agreement between the data and the model. Because of the difference in the temperature response rate and levels for the central and lateral thermocouples, the variables have been left in dimensional form.

At the smaller deformation ($\lambda = 1.03$), α_{33} is found to be 0.116 mm^2/s, which is within 2.4 percent of the value measured with the one-dimensional test and within the standard deviation of both tests. The in-plane values are found to be 0.151 and 0.153 mm^2/s, which are about 31 percent higher than α_{33}. As was suggested by the results of Doss and Wright [16] for PVC, this is likely the result of extrusion processes during the manufacturing of the neoprene sheets. Indeed, Choy et al. [27] found an increased diffusivity in the draw direction and decreased diffusivity in the direction normal to the draw of highly drawn polyethylene using a one-dimensional flash method. At the larger deformation ($\lambda = 1.52$), the mean value of α_{33} is found to be 0.112 mm^2/s, about 5.9 percent lower than the undeformed value. In contrast, the in-plane values increase to 0.165 and 0.159 mm^2/s. It should be noted that the specimen appeared to be partially translucent to the flash energy at the stretched state. This leads to error in the indicated value of α_{33} because the boundary value problem used to determine α_{33} from the temperature history is no longer strickly valid. If such error is small, it reveals itself by the indicated value of α_{33} changing as the fraction of the temperature history used in data reduction increases. Taylor [24] showed that in such circumstances the value of α_{33} may be found by extrapolating the indicated values of α_{33} calculated using different fractions of the temperature history to the one indicated at zero fraction of the temperature history. This method of correction was employed at the high stretch states. The values of α_{11} and α_{22} remained independent of the fraction of the temperature history used in data reduction because they are strongly dependent on the temperature histories of the thermocouples that are outside the projection of the aperture opening.

Conclusions

The ability to measure the multiaxial mechanical response of elastomers, and similarly planar soft tissues, promises more complete data for the formulation of constitutive models for finite strain thermomechanics. The active control of the finite deformation, via the real-time video feedback to the motor controllers, allows measurement of the material response to a wide variety of deformations that theory reveals would be useful. The equibiaxial, proportional, and constant stretch tests discussed here have illustrated this capability. Reprogramming the motor control algorithm would allow constant invariant (cf. [12]) and other tests to be easily performed, as well. Data from such multiaxial tests are not readily available in the literature.

Formulating models of general thermoelastic response requires that the temperature field within the material also be modeled. To this end, this device incorporates an extension of the flash thermal diffusivity technique that allows measurement of the in-plane components of diffusivity as well as the more commonly measured out-of-plane component. Data presented illustrate that neo-

prene rubber at low stretches may still have anisotropic thermal diffusivity and that these values may change with stretch, even over the moderate range of equibiaxial stretches examined. Such coupling may be more marked for other materials, particularly, elastomeric composites and soft tissues.

Acknowledgments

Support from the Army Research Office through grant DAAH04-95-2-2 (to JDH and NTW) as part of a Center of Excellence Award for Materials (A. S. Khan, Director) and from the Whitaker Foundation (to NTW) through a Biomedical Engineering Research Grant made this work possible. The authors would also like to thank Dr. M. G. da Silva who designed the first generation, manually controlled device.

Appendix A

Analysis of the Temperature History. In the flash method as originally developed, the top face of a planar specimen is uniformly illuminated by an impulse ([17]). The temperature field is then described by a simplified Eq. (4) as

$$\frac{\partial T}{\partial t}=\alpha_{33}\frac{\partial^2 T}{\partial x_3^2} \tag{A1}$$

where $x_3\in[0,d]$, d is the current thickness, and the subscript 3 indicates the out-of-plane direction. Neglecting convective losses, a good assumption in the short time of most one-dimensional measurements, the solution of Eq. (*A*1) for the temperature rise at the rear surface of the specimen that has experienced such a uniform impulse is ([28])

$$T(d,t)=\frac{Q}{\rho c_F d}\left[1+\sum_{n=1}^{\infty}(-1)^n\exp\left(-\frac{n^2\pi^2}{d^2}\alpha_{33}t\right)\right] \tag{A2}$$

where Q is the area-density of energy associated with a pulse of radiant energy that is assumed to be instantaneously and uniformly absorbed in a thin layer at the top face of the specimen. Noticing that the bottom face temperature history contains the parameter $\gamma=(\pi^2\alpha_{33}t/d^2)$, this solution provides a simple expression for determining α_{33} from a single point on the temperature history curve defined by Eq. (*A*2). Choosing $t_{1/2}$ as the time at which the temperature reaches one-half its maximum value $T_{\max}=Q/\rho c_F d$ yields $\gamma=1.38$. The result is

$$\alpha_{33}=\frac{1.38d^2}{\pi^2 t_{1/2}}. \tag{A3}$$

An alternative analysis, that is also employed here, is to use a Marquardt algorithm ([29]) to estimate α_{33} by minimizing the difference between a measured temperature history and results of a finite difference solution of Eq. (*A*1). The advantage of this approach is that the assumed boundary conditions may be relaxed to include possible convective losses and a finite light pulse.

Moreover, an analytical solution is not practical for determining the components of $\boldsymbol{\alpha}$ in the three-dimensional tests. Instead, the Marquardt algorithm is used again, now in conjunction with a finite difference solution of Eq. (4) written for the principal directions of the specimen. The in-plane edges of the specimen are assumed to be adiabatic because the temperature history needed to determine the components of $\boldsymbol{\alpha}$ is shorter than the time required for a significant temperature rise at these edges. A convective boundary is specified on the top face, except under the aperture opening, where a spatially uniform, time-varying heat flux is specified during the flash and followed by a convective boundary condition afterwards. The bottom boundary assumes conduction into the air underneath the specimen. Conduction in the air layer underneath the specimen plays a significant role in the temperature history at the transverse thermocouple locations of specimens of moderate thermal diffusivity (such as the range of 0.11 to 0.16 mm^2/s measured here). Recall that the aperture opening is 10 mm on a side and the distance between the central and transverse thermocouples in 15 mm, but $d\approx 3$ mm. Furthermore, the thermal diffusivity of air at room temperature is 22.5 mm^2/s as compared with the neoprene with 0.12 mm^2/s. Thus, once the air has been heated by the central region of the bottom face of the specimen, it provides an alternative path for energy transport. Since the temperature rise of the transverse thermocouples in the three-dimensional tests run here is on the order of 0.3°C, even a small addition of energy from the air can cause significant error in the determination of in-plane thermal diffusivity. The Rayleigh number is small enough to indicate the absence of buoyancy-driven flows in the air underneath the specimen ([30]). This was confirmed by measurements of the temperature response of the air and comparison with finite difference modeling. Calculated specimen temperature histories were unchanged for included air layers thicker than 13 mm.

The Marquardt algorithm and finite difference model estimate five parameters: the three components of thermal diffusivity (α_{11}, α_{22}, and α_{33}), the scaled heat flux to the specimen as defined by $q''_{\max}/\rho C$, and a convective heat loss term defined as $2hdt/\rho C dx$, where dx is the node spacing and dt the time-step. Further details are available in Doss and Wright [16].

Appendix B

Strain Measurement. Assuming a homogeneous deformation in the central region, the in-plane components of **F** can be found via ([18])

$$F_{11}=1+\frac{\partial u_1}{\partial X_1}\quad F_{12}=\frac{\partial u_1}{\partial X_2} \tag{B1}$$

$$F_{21}=\frac{\partial u_2}{\partial X_1}\quad F_{22}=1+\frac{\partial u_2}{\partial X_2} \tag{B2}$$

where u_i and X_i are the components of the displacement ($=x_i-X_i$) and original position vectors, respectively. The displacement gradients $\partial u_i/\partial X_i$ can be found via a bilinear isoparametric interpolation of any four markers that define a quadrilateral. For example, let

$$X_i=\sum_{j=1}^{n} f^j(\zeta,\eta)X_i^j \tag{B3}$$

$$u_i=\sum_{j=1}^{n} f^j(\zeta,\eta)u_i^j \tag{B4}$$

where $n\ (=4)$ denotes the number of markers and

$$f^j(\zeta,\eta)=\frac{1}{4}(1+\zeta\zeta^j)(1+\eta\eta^j) \tag{B5}$$

is a standard bilinear interpolation. In the case of equibiaxial extension (with no rotations), $F_{11}=\lambda$, $F_{22}=\lambda$ and $F_{12}=F_{21}=0$.

References

[1] Wright, N. T., Chen, S., and Humphrey, J. D., 1998, ''Time-Temperature Equivalence Applied to Heat-Induced Changes of Cells and Proteins,'' ASME J. Biomech. Eng., **120**, pp. 22–26.

[2] Truesdell, C., and Noll, W., 1965, ''The Nonlinear Field Theories of Mechanics,'' *Handbuch der Physik*, Vol. III/3, S. Flugge, ed., Springer-Verlag, Berlin.

[3] Bowen, R. M., 1989, *Introduction to Continuum Mechanics for Engineers*, Plenum Press, New York.

[4] Chadwick, P., and Creasy, C. F. M., 1984, ''Modified Entropic Elasticity of Rubber-Like Materials,'' J. Mech. Phys. Solids, **32**, No. 5, pp. 337–357.

[5] Haslach, Jr., H. W., and Zheng, N., 1995, ''Thermoelastic Generalization of Isothermal Elastic Constitutive Models for Rubber-like Materials,'' Rubber Chem. Technol., **69**, pp. 313–324.

[6] Mormon, Jr., K. N., 1995, ''A Thermomechanical Model for Amorphous Polymers in the Glassy, Transition and Rubbery Regions,'' *Recent Research in Thermo-mechanics of Polymers in the Rubbery-Glassy Range*, M. Negahban, ed., pp. 89–114, ASME, New York, pp. 89–114.

[7] Ogden, R. W., 1992, ''On the Thermoelastic Modeling of Rubber-Like Solids,'' J. Thermal Stress, **15**, pp. 533–557.
[8] Allen, G., Bianchi, U., and Price, C., 1963, ''Thermodynamics of Elasticity of Natural Rubber,'' Trans. Faraday Soc., **59**, pp. 2493–2502.
[9] Allen, G., Kirkham, M. J., Padget, J., and Price, C., 1971, ''Thermodynamics of Rubber Elasticity at Constant Volume,'' Trans. Faraday Soc., **67**, pp. 1278–1292.
[10] Anthony, R. L., Caston, R. H., and Guth, E., 1942, ''Equations of State for Natural and Synthetic Rubber-Like Materials I. Unaccelerated Natural Rubber,'' J. Phys. Chem., **46**, pp. 826–840.
[11] Shen, M. C., McQuarrie, D. A., and Jackson, J. L., 1967, ''Thermoelastic Behavior of Natural Rubber,'' J. Appl. Phys., **38**, No. 2, pp. 791–797.
[12] Humphrey, J., and Rajagopal, K. R., 1998, ''Finite Thermoelasticity of Constrained Elastomers Subject to Biaxial loading,'' J. Elast., **49**, pp. 189–200.
[13] Rivlin, R. S., and Saunders, D. W., 1951, ''Large Elastic Deformations of Isotropic Materials VII. Experiments on the Deformation of Rubber,'' Philos. Trans. R. Soc. London, Ser. A, **243**, pp. 252–288.
[14] Dashora, P., 1994, ''A Study of Variation of Thermal Conductivity of Elastomers With Temperature,'' Phys. Scr., **49**, pp. 611–614.
[15] Treloar, L. R. G., 1975, *The Physics of Rubber Elasticity*, 3rd Ed., Clarendon, Oxford, UK.
[16] Doss, D. J., and Wright, N. T., 2000, ''Simultaneous Measurement of the Orthogonal Components of Thermal Diffusivity in PVC Sheet,'' ASME J. Heat Transfer, **122** in press.
[17] Parker, W. J., Jenkins, R. J., Butler, C. P., and Abbott, G. L., 1961, ''Flash Method of Determining Thermal Diffusivity, Heat Capacity and Thermal Conductivity,'' J. Appl. Phys., **32**, No. 9, pp. 1679–1684.
[18] Humphrey, J. D., Vawter, D. L., and Vito, R. P., 1987, ''Quantification of Strains in Biaxially Tested Soft-Tissues,'' J. Biomech., **20**, No. 1, pp. 59–65.
[19] Wright, N. T., da Silva, M. G., Doss, D. J., and Humphrey, J., 1995, ''Measuring Thermal Properties of Elastomers Subject to Finite Strain,'' *Thermal Conductivity 23*, K. E. Wilkes et al., eds., Technomic, Lancaster, PA, pp. 639–646.
[20] Downs, J., Halperin, H. R., Humphrey, J. D., and Yin, F. C. P., 1990, ''An Improved Video-based Computer Tracking System for Soft-Biomaterials Testing,'' IEEE Trans. Biomed. Eng., **37**, pp. 903–907.
[21] Agari, Y., Ueda, A., and Nagai, S., 1994, ''Measurement of Thermal Diffusivity and Specific Heat Capacity of Polymers by Laser Flash Method,'' J. Polym. Sci., Part B: Polym. Phys., **33**, pp. 33–42.
[22] Lachi, M., and Degiovanni, A., 1991, ''Determination des Diffusivites Thermiques des Materiaux Anisotropes par Methode Flash Bidirectionelle,'' J. Phys. III, No. 12, pp. 2027–2046.
[23] Mallet, D., Lachi, M., and Degiovanni, A., 1990, ''Simultaneous Measurements of Axial and Radial Thermal Diffusivities of an Anisotropic Solid in Thin Plate: Application to Multi-Layered Materials,'' *Thermal Conductivity 21*, C. J. Cremers and H. A. Fine, eds., Plenum Press, New York, pp. 91–107.
[24] Taylor, R. E., 1975, ''Critical Evaluation of Flash Method for Measuring Thermal Diffusivity,'' Rev. Int. Hautes Temp. Refract., **12**, pp. 141–145.
[25] Kawabata, S., and Kawai, H., 1977, ''Strain Energy Function of Rubber Vulcanizates From Biaxial Extension,'' Adv. Polym. Sci., Vol. 24, H. J. Cantow et al., Springer-Verlag, New York, pp. 89–124,
[26] Obata, Y., Kawabata, S., and Kawai, H., 1970, ''Mechanical Properties of Natural Rubber Vulcanizates in Finite Deformation,'' J. Polym. Sci., Part A: Gen. Pap., **8**, pp. 903–919.
[27] Choy, C. L., Luk, W. H., and Chen, F. C., 1978, ''Thermal Conductivity of Highly Oriented Polyethylene,'' Polymer, **19**, pp. 155–162.
[28] Carslaw, H. S. and Jaeger, J. C., 1959, *Conduction of Heat in Solids*, 2nd Ed., Clarendon Press, Oxford, UK.
[29] Press, W. H., Teukolsky, S. A., Vetterling, W. T., and Flannery, B. P., 1992, *Numerical Recipes in C*, Cambridge University Press, Cambridge, UK.
[30] Gebhart, B., Jaluria, Y., Mahajan, R. L., and Sammukia, B., 1988, *Buoyancy-Induced Flows and Transport*, Hemisphere, New York.